Inorg. Chem. **2008**, *47*, 7757−7767

Investigation of Nanostructure and Thermal Behavior of Zinc-Substituted Fluorapatite

G. W. Chinthaka Silva,*,†,‡ Oliver Hemmers,† Ken R. Czerwinski,†,‡ and Dennis W. Lindle†

Department of Chemistry, University of Nevada, Las Vegas, Nevada 89154-4003, and Harry Reid Center for Environmental Studies, University of Nevada, Las Vegas, Box 454009, 4505 Maryland Parkway, Las Vegas, Nevada 89154

Received April 30, 2008

The incorporation of various cations such as Zn^{2+} into the structure of fluorapatite, $Ca_5(PO_4)_3F$, is governed by the effectiveness of the cations to substitute for Ca^{2+} ions. In this work different concentrations of zinc were used to substitute for calcium. Microscopic characterization was done by observing the nanostructural variations induced by these zinc substitutions and by relating these observations to thermal behavior of the zinc-substituted fluorapatite. Random incorporation of zinc into the fluorapatite structure and the zinc induced amorphization effects oriented in the nanostructure of fluorapatite led to phase impurities of zinc-substituted fluorapatites when the amount of zinc used was greater than 25 mol % of the total cation concentration. It also was observed that the thermal stability of the samples decreased with increasing zinc concentration. Among the zinc-incorporated samples, the most similar chemical and physical properties to the single-phased fluorapatite were identified in the sample containing the lowest amount of zinc (25 mol %). After calcination, however, this sample showed to contain some defects in the atomic arrangement of the nanostructure which led to a thermal instability of the fluorapatite.

1. Introduction

Among a number of ceramic waste forms considered for loading high-level nuclear wastes, fluorapatite is known to have moderate resistance to the ion-induced amorphization.[1,2] Ceramic waste forms are important because the waste load they can bear is greater than that of conventional glass-type nuclear waste forms.[3] One of the important aspects in considering the durability of nuclear waste-form materials is the materials' ability to retain the radionuclides within the waste form. Fluorapatite has shown some promising results for this purpose.[4] It is also important that the waste form sustain its crystallinity[5,6] under radiation damage and repository conditions. If the crystallinity of the waste form is compromised, radionuclides could leach into the environment.[4] Chaumont et al. [1] also showed it is necessary to have annealing conditions of the fluorapatite waste form in order for the crystallinity to be preserved, and these conditions could be partially found with materials containing the α-emitting radionuclides. However, structural modifications of fluorapatite might be needed to load a considerable amount of actinides[1] because the substitution sometimes leads to unexpected crystal structure changes.[7] Furthermore, group 2 elements, such as Sr, are constituents of high-level waste and would be incorporated into a calcine waste form.[3] This work will examine the impact that Zn, a d^{10} divalent element, has on waste-form characteristics. In addition to the electronic structure variations, Zn has a substantially smaller ionic radius of 0.60 Å compared to either Ca (1.00 Å) or Sr (1.18 Å).[8] It is known that Zn has low substitution for Ca in hydroxyapatite.[9] Others have demonstrated that Sr can com-

* To whom correspondence should be addressed. E-mail: silvag2@unlv.nevada.edu. Tel: (702) 895 4123. Fax: (702) 895 3094.
† Department of Chemistry.
‡ Harry Reid Center for Environmental Studies.

(1) Chaumont, J.; Soulet, S.; Krupa, J. C.; Carpena, J. *J. Nucl. Mater.* **2002**, *301*, 122.
(2) Meldrum, A.; Wang, L. M.; Ewing, R. C. *Nucl. Instrum. Methods Phys. Res., Sect. B.* **1996**, *116*, 220.
(3) Raman, S. V. *J. Mater. Sci.* **1998**, *33*, 1887.
(4) Miro, S.; Studer, F.; Costantini, J. M.; Berger, P.; Haussy, J.; Trouslard, P.; Grob, J. J. *J. Nucl. Mater.* **2007**, *362*, 445.
(5) Sickafus, K. E.; Minervini, L.; Grimes, R. W.; Valdez, J. A.; Ishimaru, M.; Li, F.; McClellan, K. J.; Hartmann, T. *Science.* **2000**, *289*, 748.
(6) Sickafus, K. E.; Grimes, R. W.; Valdez, J. A.; Cleave, A.; Tang, M.; Ishimaru, M.; Corish, S. M.; Stanek, C. R.; Uberuaga, B. P. *Nat. Mater.* **2007**, *6*, 217.
(7) Rakovan, J.; Reeder, R. J.; Elzinga, E. J.; Cherniak, D. J.; Tait, C. D.; Morris, D. E. *Environ. Sci. Technol.* **2002**, *36*, 3114.
(8) Shannon, R. D. *Acta Crystallogr.* **1976**, *A32*, 751.
(9) Bigi, A.; Foresti, E.; Gandolfi, M.; Gazzano, M.; Roveri, N. *J. Inorg. Biochem.* **1995**, *58*, 49.

10.1021/ic800794x CCC: $40.75
Published on Web 08/05/2008

Table 1. Synthesized Samples as a Function of Ca/(Ca + Zn) Molar Ratios Used

sample	$Ca(NO_3)_2 \cdot 4H_2O$	$Zn(NO_3)_2$	Ca/(Ca + Zn) molar ratio (%)	expected chemical composition
Fap	0.08		1	$Ca_5(PO_4)_3F$
25ZnAp	0.06	0.02	0.75	$Ca_{3.75}Zn_{1.25}(PO_4)_3F$
50ZnAp	0.04	0.04	0.50	$Ca_{2.50}Zn_{2.50}(PO_4)_3F$
75ZnAp	0.02	0.06	0.25	$Ca_{1.25}Zn_{3.75}(PO_4)_3F$
ZnAp	0.08		0.00	$Zn_5(PO_4)_3F$

pletely exchange with Ca in fluorapatite.[10] Therefore, other than having α-emitting nuclear waste in the waste form, it is also important to investigate amorphization effects on the calcine waste-form based on the fundamental chemistry of the elements, in this case the ionic radius and the electronic properties.

The fluorapatite crystalline structure contains four non-equivalent ions (F^-, PO_4^{3-}, Ca_I^{2+}, and Ca_{II}^{2+}) with their unique space-phase orientations.[11] This crystallography of fluorapatite enables other ions to exchange with these four non-equivalent ions.[12] In the case of calcium substitution, one or both Ca^{2+} sites may be replaced with an incorporating cation depending on the nature of the substituting ion.[13−16] In some cases, the concentration level of cation substitution inhibits fluorapatite crystallization.[17] However, sintering the samples overcomes these crystallization-inhibition effects, enabling the fluorapatite to act as a suitable host of the substituting ions.[17] Some impurities, such as CaF_2, can form eutectics, depressing the fluorapatite melting point.[17−19] These observations suggest that it is important to evaluate the crystallography and thermal stability of fluorapatite toward the substitution of other ions, with this work examining the impact of nanostructure of divalent cations. Here, the incorporation of zinc into fluorapatite by introducing Zn^{2+} cations into the precipitation solution[17] and the zinc-incorporation effects on the crystallinity and the thermal stability of fluorapatite are presented by observing nanostructural characteristics of the samples. The morphology and nanostructure of zinc-containing fluorapatite are examined using microscopic techniques such as scanning electron microscopy (SEM) and transmission electron microscopy (TEM). Such methods have proven useful in other studies on fluorapatite nanostructure.[20]

2. Experimental Details

2.1. Synthesis of Powder Samples. A wet method[17] was used to synthesize fluorapatite and Zn-containing fluorapatites. The source compounds used for Ca^{2+}, Zn^{2+}, PO_4^{3-}, and F^- were $Ca(NO_3)_2 \cdot 4H_2O$, $Zn(NO_3)_2$, $(NH_4)_2HPO_4$, and NH_4F, respectively. These chemicals were used in stoichiometric ion solutions of Ca^{2+}, PO_4^{3-}, and F^- ($Ca^{2+}/PO_4^{3-}/F^- = 5:3:1$ molar ratio) to synthesize fluorapatite. Incorporation of zinc was performed by introducing Zn^{2+} ions into the Ca^{2+} cation solution. The concentration of zinc used for the apatite synthesis was varied, changing the zinc ion concentration in the final cationic solution. The final stoichiometry, $(Ca^{2+} + Zn^{2+})/PO_4^{3-}/F^- = 5:3:1$, of the samples was maintained using the appropriate amounts of each compound. The relative concentration of zinc to calcium varied from 25 to 100 atomic percentages in four steps so that the final Zn/Ca atomic percentages were 25, 50, 75, and 100%.

A solution mixture of $(NH_4)_2HPO_4$ and NH_4F was brought to boil, and a second solution containing the cations (Ca^{2+} or Ca^{2+} and Zn^{2+}) was added. The pH of the reaction mixture was increased to 9.0 by adding concentrated ammonia. The solution was stirred vigorously for 3 h, and the pH was maintained by adding ammonia. After stirring, the precipitate that formed was filtered and washed thoroughly with distilled water. Residual water trapped in the precipitate was removed by heating the sample overnight at 70 °C. The synthesized powder sample was then used for the characterization, calcinations, and for sintering (Table 1).

2.2. Characterization Methods. Chemical phases of the powder samples were identified by X-ray powder diffraction (XRD) using a Philips PANalytical instrument with a 40 kV X-ray Cu target and a Ni filter. Rietveld analysis was used to refine the lattice parameters using approximate crystal structures from the Inorganic Crystallographic Structure Database (ICSD). SEM and TEM were used for morphological and nanostructural studies. SEM imaging was performed on a JEOL SEM model JSM-5610 equipped with secondary electron (SE) and backscattered electron (BE) detectors and an Oxford ISIS EDS (energy dispersive spectroscopy) system. Furthermore, elemental analysis of the as-synthesized samples was performed by EDS. A TECNAI-G2-F30 TEM with a 300 keV Schottky field-emission gun was used for TEM imaging. Sample

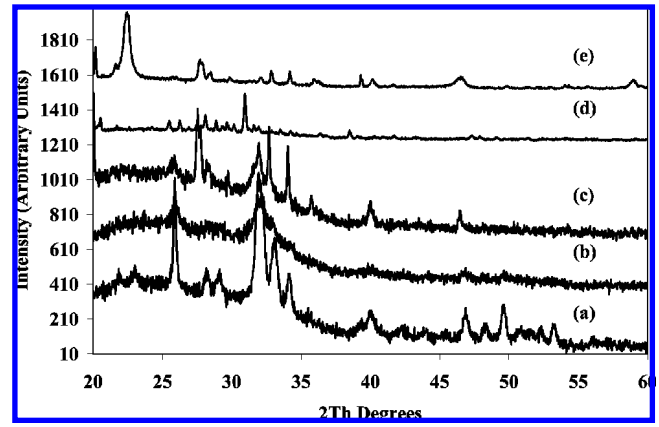

Figure 1. XRD patterns of the as-synthesized samples: (a) Fap; (b) 25ZnAp; (c) 50ZnAp; (d) 75ZnAp; (e) ZnAp.

Table 2. Chemical Phases Identified in the As-Synthesized Samples from Their XRD Patterns

sample	chemical phases			
	primary phase	secondary phases		
Fap	$Ca_5(PO_4)_3F$			
25ZnAp	$Ca_5(PO_4)_3F$			
50ZnAp	$Ca_5(PO_4)_3F$	NH_4ZnPO_4		
75ZnAp	NH_4ZnPO_4	$Zn_3(PO_4)_2$	$Ca_3(PO_4)_2$	$CaZn_2(PO_4)_2$
ZnAp	NH_4ZnPO_4	$Zn_3(PO_4)_2$		

(10) Hill, R. G.; Stamboulis, A.; Law, R. V.; Clifford, A.; Towler, M. R.; Crowley, C. *J. Non-Cryst. Solids.* **2004**, *336*, 223.
(11) Leroy, N.; Bres, E. *Eur. Cells Mater.* **2001**, *2*, 36.
(12) Calderin, L.; Stott, M. J. *Phys. Rev. B.* **2003**, *67*, 134106.
(13) Terra, J. *Philos. Mag. A.* **2002**, *82*, 2357.
(14) Tamm, T.; Peld, M. *J. Solid State Chem.* **2006**, *179*, 1581.
(15) Manecki, M.; Maurice, P. A.; Traina, S. J. *Am. Mineral.* **2000**, *85*, 932.
(16) Rakovan, J. F.; Hughes, J. M. *Can. Mineral.* **2000**, *38*, 839.
(17) Hidouri, M.; Bouzouita, K.; Kooli, F.; Khattech, I. *Mater. Chem. Phys.* **2003**, *80*, 496.
(18) Ayed, F. B.; Bouaziz, J.; Bouzouita, K. *J. Alloys Compd.* **2001**, *322*, 238.
(19) Ayed, F. B.; Bouaziz, J.; Bouzouita, K. *J. Eur. Ceram. Soc.* **2000**, *20*, 1069.
(20) Silva, G. W. C.; Ma, L.; Hemmers, O.; Lindle, D. *Micron* **2007**, *39*, 269.

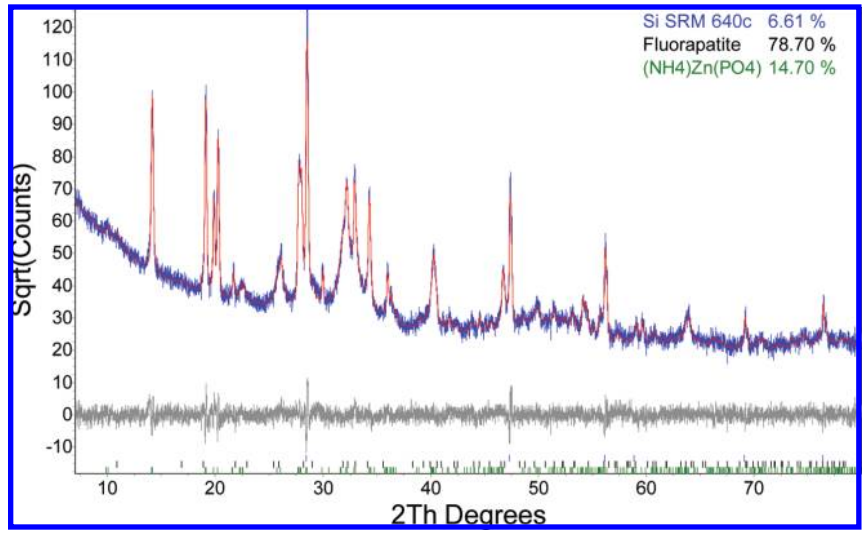

Figure 2. XRD/Rietveld analysis of the 50ZnAp sample. Experimental and calculated patterns are shown in blue and red colors, respectively. The Rwp for the fit is 9.1%.

Table 3. Lattice Parameters of the Fluorapatite Chemical Phase of the As-Synthesized Fap, 25ZnAp, and 50ZnAp Samples

	Fap	25ZnAp	50ZnAp
a (Å)	9.378(1)	9.364(2)	9.391(3)
c (Å)	6.882(1)	6.832(1)	6.864(3)
V (Å^3)	524.4(1)	521.6(5)	524.2(4)

Table 4. Elemental Analysis of the As-Synthesized Samples

	averaged atom percentages (%)				
element	Fap	25ZnAp	50ZnAp	75ZnAp	ZnAP
O K (±1.25)	67.8	65.5	69.0	70.0	61.4
F K (±1.26)	11.3	11.8	9.2	7.6	7.8
P K (±1.47)	7.9	7.9	9.2	10.9	12.2
Ca K (±1.27)	13.0	13.0	10.0	4.8	
Zn K (±0.71)		1.9	2.6	6.7	18.6
(Ca + Zn)/P molar ratio	1.6	1.9	1.4	1.1	1.5

specimens for TEM observations were prepared using a solution-drop method[20] in which the ground sample was mixed in ethanol and sonicated for 10 min to homogenize the particle distribution. Thermogravimetric analysis (TGA) and differential scanning calorimetric (DSC) profiles were obtained utilizing a NETZSCH STA 449C instrument. The thermal behavior of each sample was studied in the 25 to 500 °C temperature range using a 5 K/min heating rate.

3. Results

3.1. Characterization of the As-Synthesized Samples. XRD patterns of the as-synthesized samples are shown in Figure 1. These patterns demonstrate that only the first three samples in Table 1 have the fluorapatite chemical phase. The Fap and 25ZnAp samples have only the fluorapatite chemical phase, whereas 50ZnAp has two chemical phases: fluorapatite and ammonium zinc phosphate (Table 2). Furthermore, the Rietveld analysis performed on the XRD pattern of 50ZnAp showed that 84.3 ± 0.1 wt % is fluorapatite while the rest is a secondary phase, NH_4ZnPO_4 (Figure 2). According to the XRD patterns in Figure 1, however, the incorporation of zinc into fluorapatite decreases crystallinity of the fluorapatite phase in both 25ZnAp and 50ZnAp. Formation of the NH_4ZnPO_4 phase is favored with increasing zinc concentration. Table 3 summarizes the crystallographic parameters of the samples determined using the XRD patterns. As-synthesized 25ZnAp has smaller lattice parameters *a* and *c* than Fap confirming the incorporation of zinc into fluorapatite. The 50ZnAp sample has a lower *c* value than the Fap sample, but the *a* value is greater than the *a* values of both Fap and 25ZnAp. Incomplete incorporation of zinc into fluorapatite (Table 4) and formation of a crystallized secondary phase are possible reasons for this behavior.

SEM micrographs of the first two samples in Figures 3a and 3b show similar bulk characteristics in their morphology, and 50ZnAp (Figure 3c) also shows some morphological similarities to Fap and 25ZnAp. However, the bulk particle morphology of 75ZnAp and ZnAp in Figures 3d and 3e, respectively, are quite different from that of Fap. Also, the crystalline characteristics are prominent in the last two samples, especially in ZnAp. Even though the particle shapes of the as-synthesized samples were not clear in SEM micrographs, TEM BF images of the sonicated microparticles show somewhat clear particle shapes (Figure 4). Fap has plate-like shapes whereas the plate-like shapes of the 25ZnAp sample particles are incomplete, and 50ZnAp has granular-like particles. The high-resolution TEM (HRTEM) image of fluorapatite (Figure 5 inset) consists of fringes of tunnel rows of 2-fold multiplicity, as shown in the intensity plot. This image also indicates that most of the focused particle area is crystalline, and the inset FFT confirms this observation as it consists of intense diffraction spots.

The HRTEM image of the 25ZnAp sample contains nanoparticle areas of different crystallinity (Figure 6). Lattice fringes in the middle area of the image have higher contrast than the areas indicated by two smaller boxes. Furthermore, these high contrast fringes have a 4-fold multiplicity, indicating high order in the crystalline lattice areas.

An HRTEM image of a different region of the 25ZnAp sample (Figure 7) indicates characteristics of another particle area that has a bulk amorphous phase. The ring patterns in the overall FFT (inset) further verify this observation. There are two lattice orientations in the crystalline area of the particle: lattice fringes are parallel to the (200) planes of

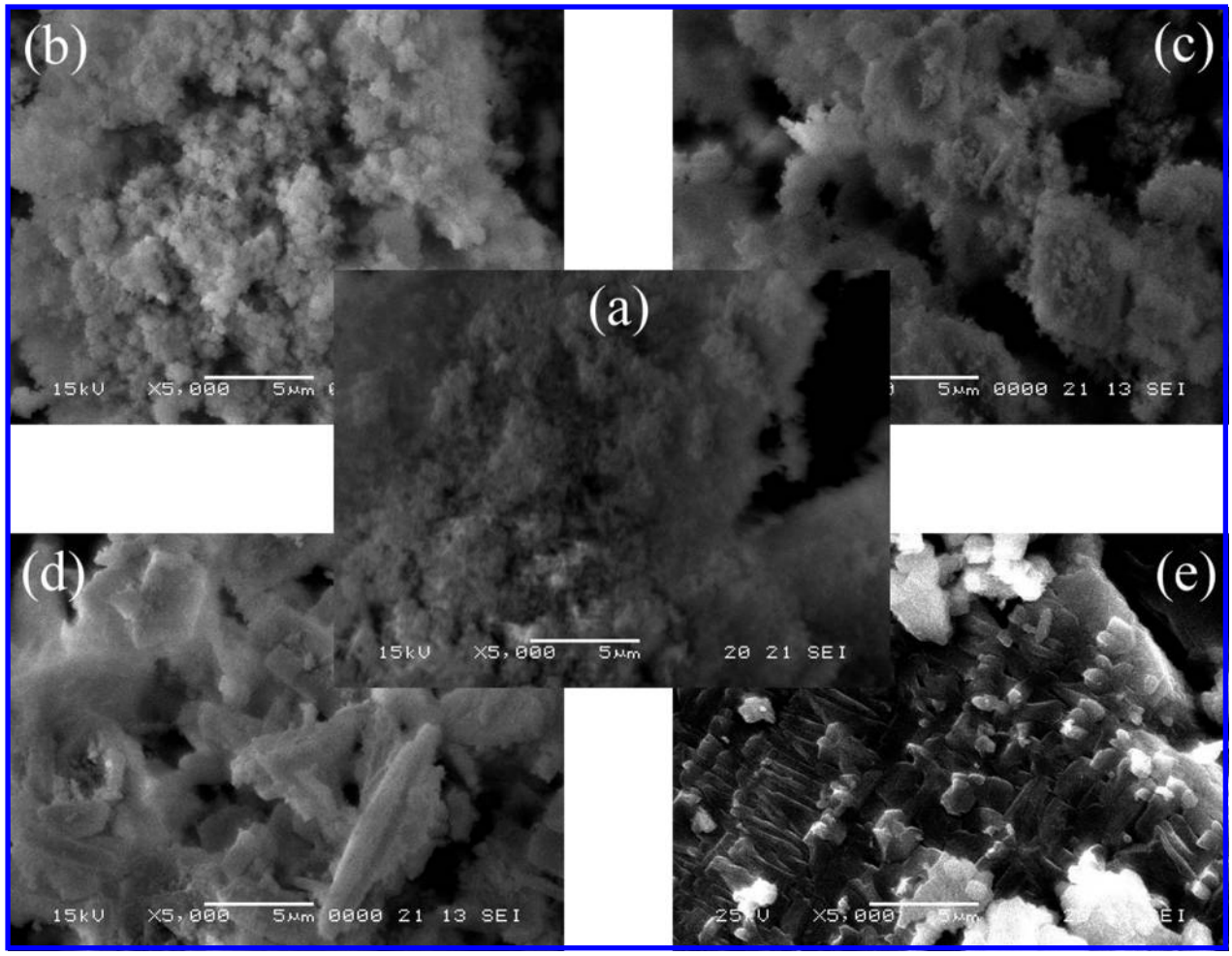

Figure 3. SEM micrographs of the as-synthesized samples: (a) Fap; (b) 25ZnAp; (c) 50ZnAp; (d) 75ZnAp; (e) ZnAp.

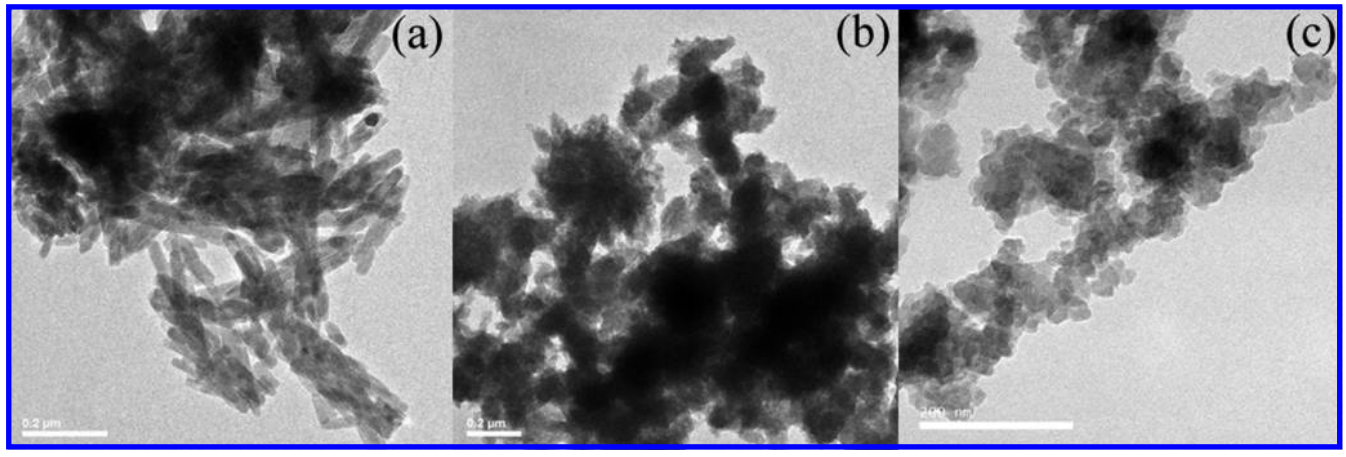

Figure 4. TEM BF images of the first three samples: (a) Fap; (b) 25ZnAp; (c) 50ZnAp.

fluorapatite in the first orientation while the second orientation corresponds to systematic reflections of (100) planes of fluorapatite. In this second area, reflections can be seen in two directions and with 3-fold multiplicity, suggesting a higher crystallinity than the first area. There are also some amorphous patches (circled) in the crystalline side of the particle, suggesting random-space orientations of amorphous and partially crystallized zinc incorporated fluorapatite.

The HRTEM image of 50ZnAp shown in Figure 8a has lattice fringes in several different orientations, and three of them are highlighted in the image. Lattice fringes in the two regions separated from the grain boundary are due to systematic reflections of fluorapatite planes along the [110] and [200] directions in the [001] beam direction. The intensity profile along A–B (Figure 8b) shows that the lattice fringes in this area have a particular order. The intensity profile along the C–D direction (Figure 8c) has 4-fold multiplicity while the lattice fringe orientation along E–F (Figure 8d) is random and is possibly due to overlapping $Ca_5(PO_4)_3F$ and NH_4ZnPO_4 grains.

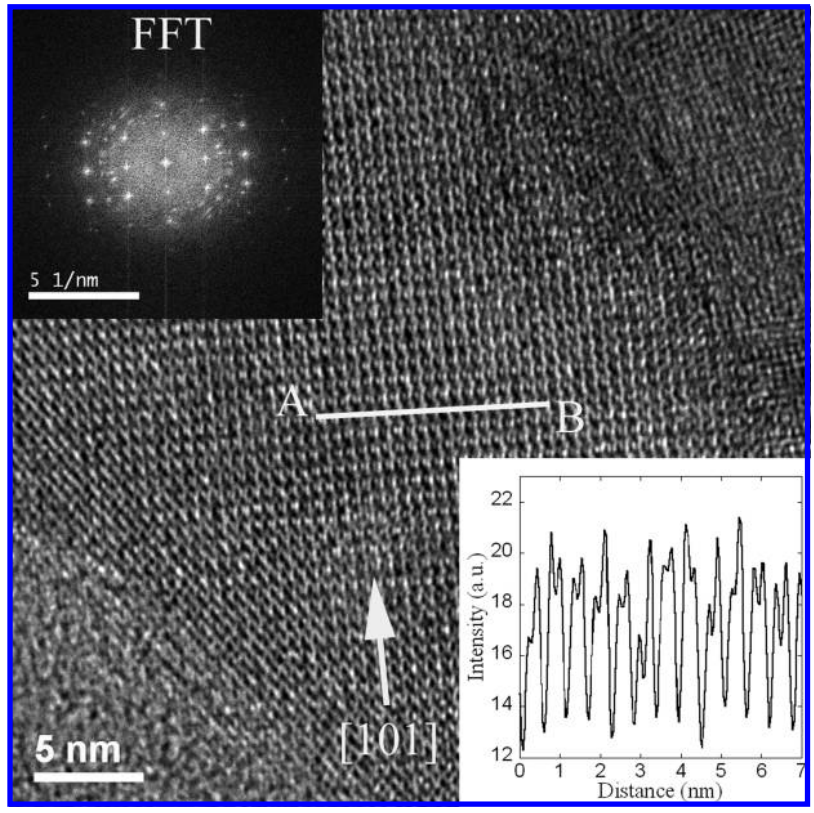

Figure 5. HRTEM image of the Fap sample along [101] direction.

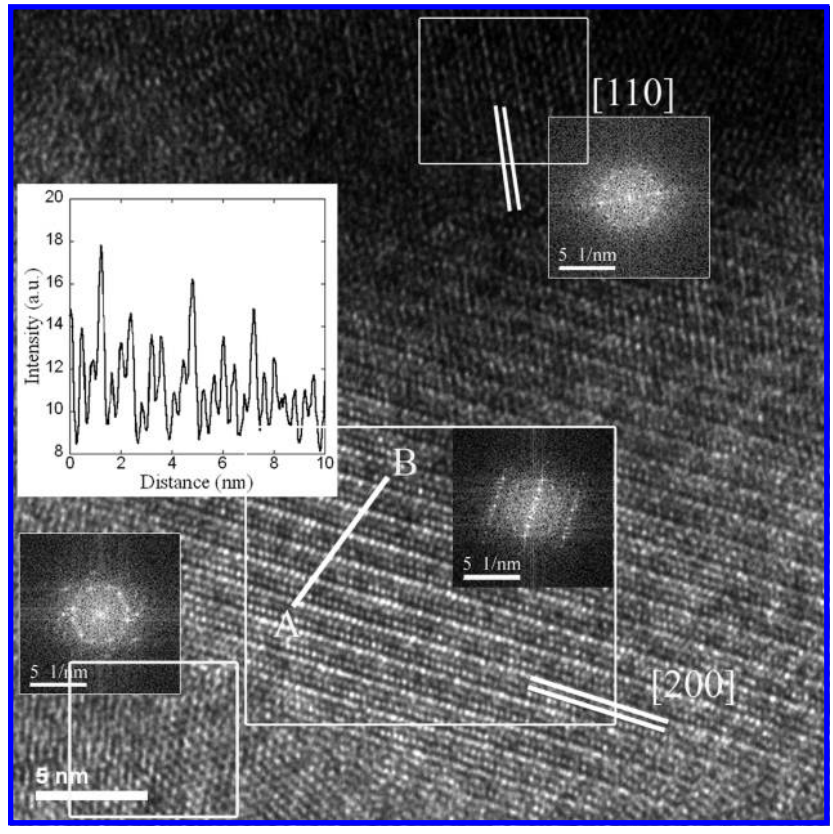

Figure 6. HRTEM image of the as-synthesized 25ZnAp sample.

3.2. Thermal Behavior. Fap and 25ZnAp samples showed a high thermal stability in the temperature range from 25 to 500 °C, while the other three samples demonstrated weight losses over the same range. These weight losses are related to different endothermic peaks in the corresponding DSC profiles (Figure 9). The endothermic peak near 125 °C in

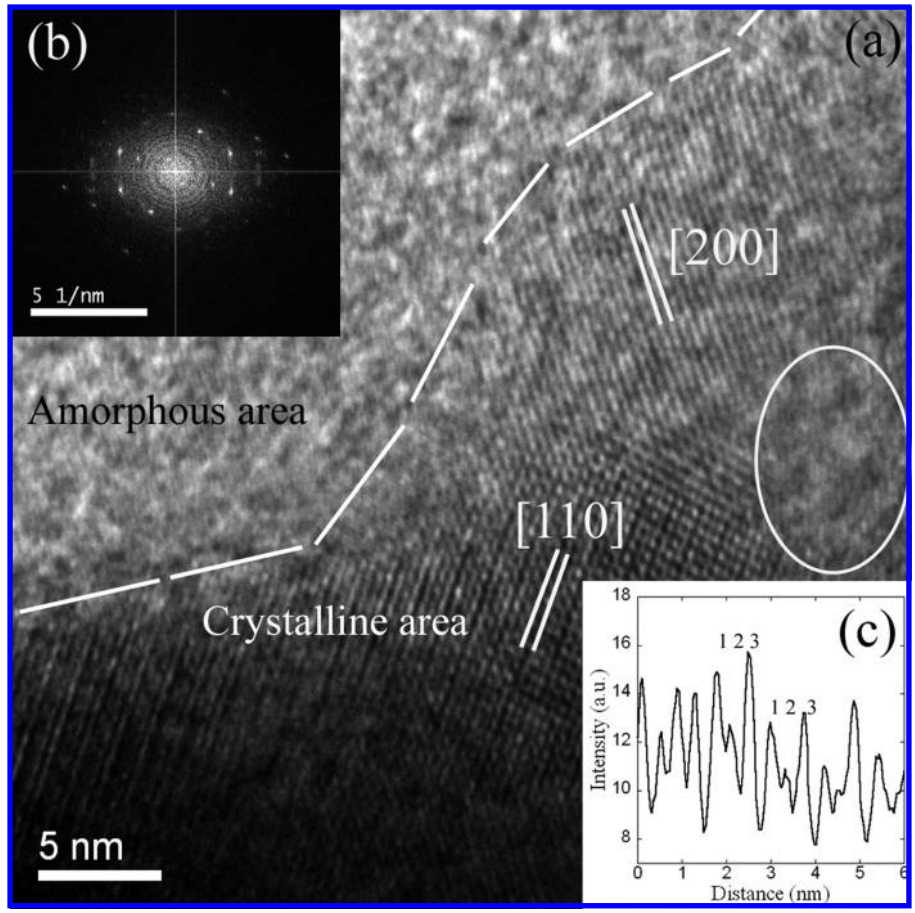

Figure 7. HRTEM image of the 25ZnAp sample in another particle area: (a) HRTEM image; (b) overall FFT micrograph; (c) intensity profile of the crystalline area normal to [110] direction.

the DSC plots of Fap and 25ZnAp samples are probably due to removal of residual water. Peaks in the other three samples could be related to decomposition of the species ammonium zinc phosphate and calcium zinc phosphates.

Figure 10 shows the percentage weight losses of the samples obtained from the thermogravimetric profiles in the 25−500 °C temperature range. In this range, the lowest weight loss is for Fap, and the weight loss increases linearly with the proportion of zinc in the synthesized compounds. Low thermal stability of the samples with large amounts of zinc may be due to the formation of secondary phases in the samples.

The chemical phases identified in the samples from their XRD patterns after calcination are given in Table 5. The Fap sample consists of a single fluorapatite phase with high crystallinity while 25ZnAp exhibits a primary fluorapatite phase and a secondary calcium zinc phosphate phase up to about 6.0 ± 0.1 wt %. However, the zinc-incorporated fluorapatite phase observed in the as-synthesized 50ZnAp sample decomposed to calcium zinc phosphates indicating a low thermal stability of the fluorapatite phase with higher zinc concentration than in the 25ZnAp sample. The 75ZnAp and ZnAp samples did not exhibit a presence of a fluorapatite chemical phase even after the calcination process. Calcined 75ZnAp consists of a major calcium zinc phosphate phase while the major phase of the calcined ZnAp is zinc phosphate.

SEM micrographs of the calcined Fap, 25ZnAp, and 50ZnAp samples are shown in Figure 11. Particle size and shape of 25ZnAp (Figure 11b) and 50ZnAp (Figure 11c) samples show similarities in the presence of zinc-substituted calcium phosphates. Fap (Figure 11a) particles have a plate-like shape with smaller particle size compared to the 25ZnAp and 50ZnAp samples. These latter two samples have both plate-like and granular characteristics. Figures 12a and 12b show TEM BF images of the calcined Fap and calcined 25ZnAp, respectively. The first image indicates that the Fap sample consists of particles with well crystallized facets. Even though a similar trend of particle shape is apparent for the 25ZnAp particles (Figure 12b), the blunt edges of the particles indicate the lower crystallinity of the sample than of the Fap. Furthermore, an increase in the 25ZnAp particle size can be seen with respect to Fap. The HRTEM fringe lineup of a 25ZnAp particle along the [110] direction is shown in Figure 13. In the upper left side of the figure, fringes have both sets of details. After each set of two fringe rows along the direction normal to the line from A to B, there is a black line of equal width separating the fringe rows. However, this separation disappears at point B where one-fold tunnel rows start to appear. The intensity profile in the figure (inset) shows this particular change in the fringe order moving along A to C through point B. Such fringe details in one direction and both directions are absent at points E and F, respectively.

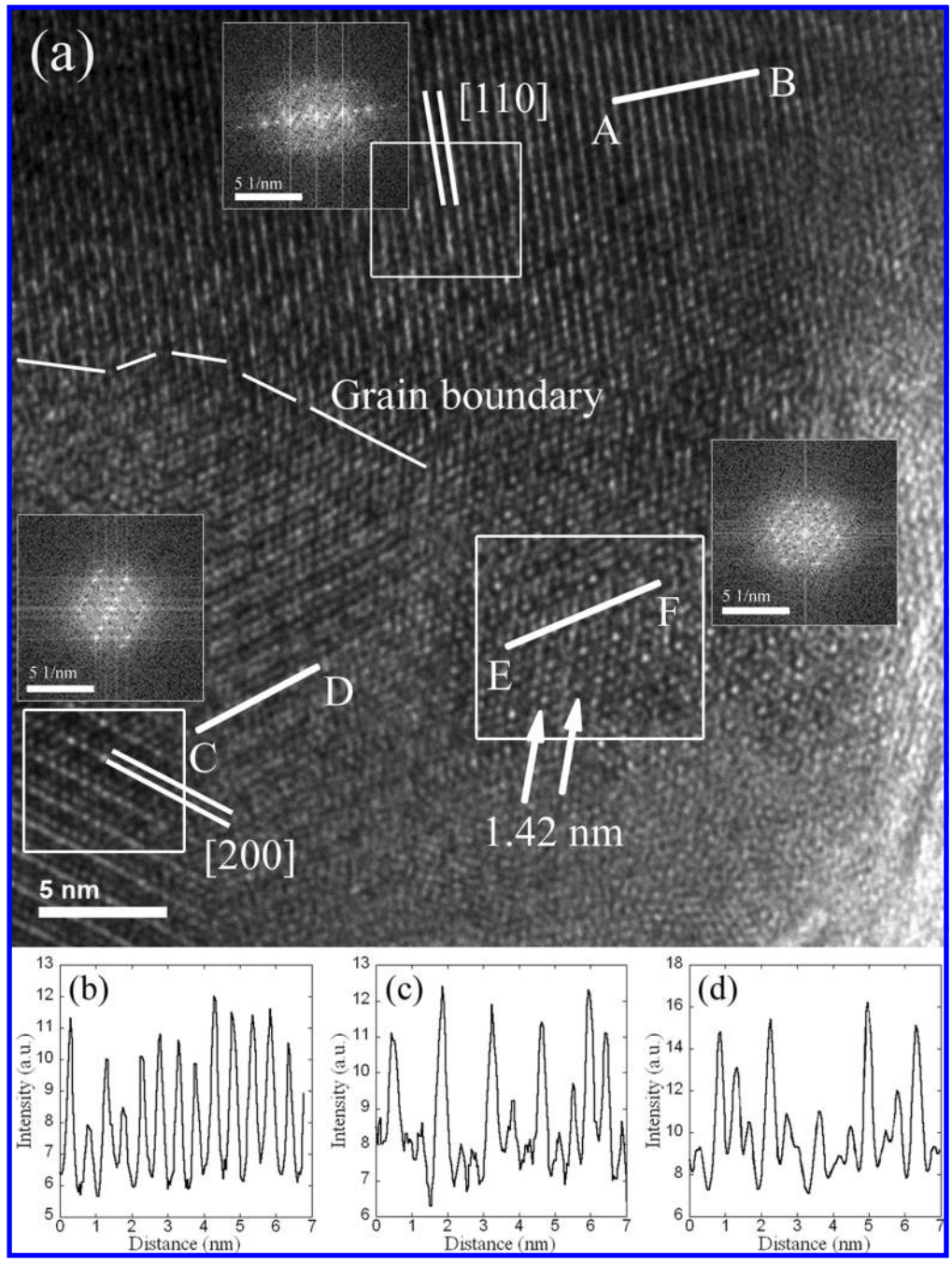

Figure 8. (a) HRTEM image of 50ZnAp sample and the intensity profiles (b) along AB, (c) along CD, and (d) along EF.

A higher order in the crystal structure of the calcined Fap sample can be seen in the HRTEM image shown in Figure 14a. There are lattice fringes of two-atom layers connected in a chain-like manner. Figure 14b is the HRTEM image of calcined 25ZnAp in which the atom layers are more separated than in Fap. There are three significantly intense atom layers in Figure 14b, and after the second row in each of these 3-fold multiplicities, there is also a low intense atom layer which can be seen only in particular areas of the image. Dislocations (highlighted by a rectangle) can also be detected in the 25ZnAp nanostructure, possibly because of stacking faults when zinc is incorporated into some of the calcium sites. There are also some locations (circle) where atoms are missing. These observations show that zinc-incorporated fluorapatite has random distributions of atomic layers in some areas of the structure and also a lower structural integrity than pure fluorapatite.

Sintering of Fap and 25ZnAp samples was performed using the as-synthesized and the calcined samples in both cases. Sintering of Fap using either the as-synthesized sample or the calcined sample yielded a secondary calcium phosphate secondary phase (Figure 15) with fluorapatite as the major phase. The sintered 25ZnAp sample showed similar chemical composition to that of the calcined sample. Furthermore, the sintering of the calcined 25ZnAp sample resulted in the decomposition of the zinc-incorporated fluorapatite phase into $Ca_{19}Zn_2(PO_4)_{14}$, with some impurity

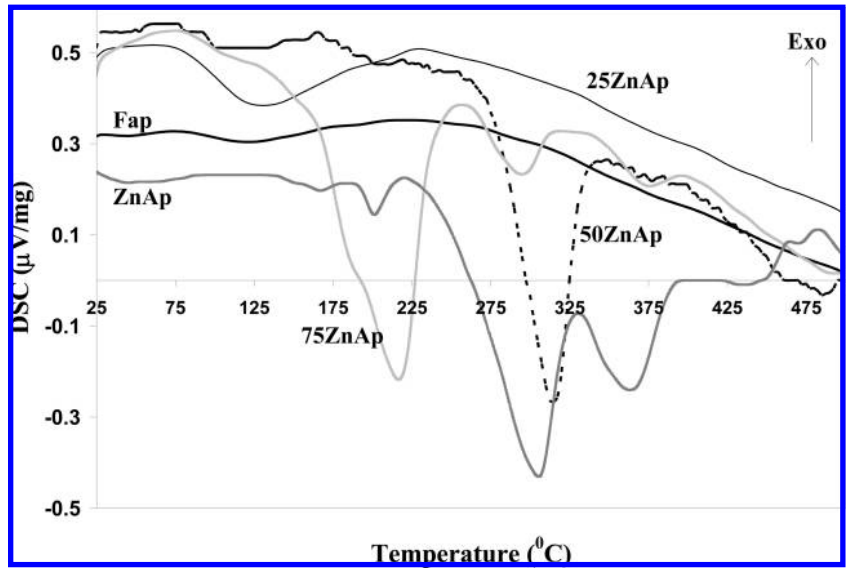

Figure 9. DSC profiles of Zn-containing fluorapatite samples.

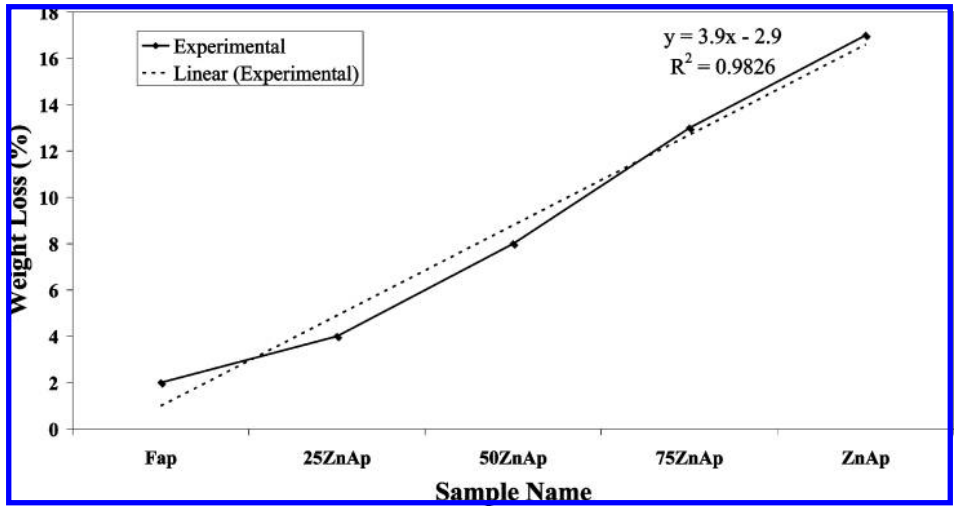

Figure 10. Weight losses of synthesized apatite samples, obtained from TGA in the temperature range 25−500 °C.

Table 5. Chemical Phases Identified in the Samples after Calcinations at 900 °C for 1 h under Air

sample	chemical phases		
	primary phase	secondary phases	
Fap	$Ca_5(PO_4)_3F$		
25ZnAp	$Ca_5(PO_4)_3F$	$CaZn_2(PO_4)_2$	
50ZnAp	$CaZn_2(PO_4)_2$	$Ca_{19}Zn_2(PO_4)_{14}$	
75ZnAp	$CaZn_2(PO_4)_2$	$Zn_3(PO_4)_2$	$Ca_3(PO_4)_2$
ZnAp	$Zn_2P_2O_7$	$Zn_3(PO_4)_2$	

peaks that correspond to calcium phosphate, especially at the 31.03° 2θ value (Figure 16).

4. Discussion

Minerals of the apatite group, such as fluorapatite, have the ability to interchange their constituents with other monovalent, divalent, and trivalent elements or chemical groups.[16,17,22] Chemical compatibility of these foreign ions to the substituting ions in fluorapatite with respect to ionic radii and oxidation state and the chemical structure of fluorapatite enable these substitutions.[11,23] Even though zinc (0.60 Å) has an ionic radius smaller than that of the calcium ion (1.00 Å),[10] XRD and other microscopic studies showed the formation of zinc-substituted fluorapatite up to the 50ZnAp sample. The flexibility of the fluorapatite chemical structure to permit other cations to substitute calcium ions would probably be the reason for this observation. However, sample crystallinity decreased with the increase in zinc concentration. Refined lattice parameters of Fap and 25ZnAp indicated that the zinc is incorporated into the fluorapatite structure. Formation of a secondary chemical phase in 50ZnAp, however, affected the lattice parameters of the fluorapatite phase. This sample was an outlier in the trend on the reduction of the fluorapatite lattice parameter with respect to an increasing concentration of zinc (Table 3).

(21) Panda, R. N.; Hsieh, M. F.; Chung, R. J.; Chin, T. S. *J. Phys. Chem. Solids* **2003**, *64*, 193.

(22) Weber, W.; Ewing, R. C.; Catlow, C. R. A.; Diazdela Rubia, T.; Hobbs, L. W.; Kinoshita, C.; Matzke, H. j.; Motta, A. T.; Nastasi, M.; Salje, E. H. K.; Vance, E. R.; Zinkle, S. J. *J. Mater. Res.* **1998**, *13*, 1434.

(23) Leroy, G.; Penel, G.; Leroy, N.; Bres, E. *Appl. Spectrosc.* **2002**, *56*, 1030.

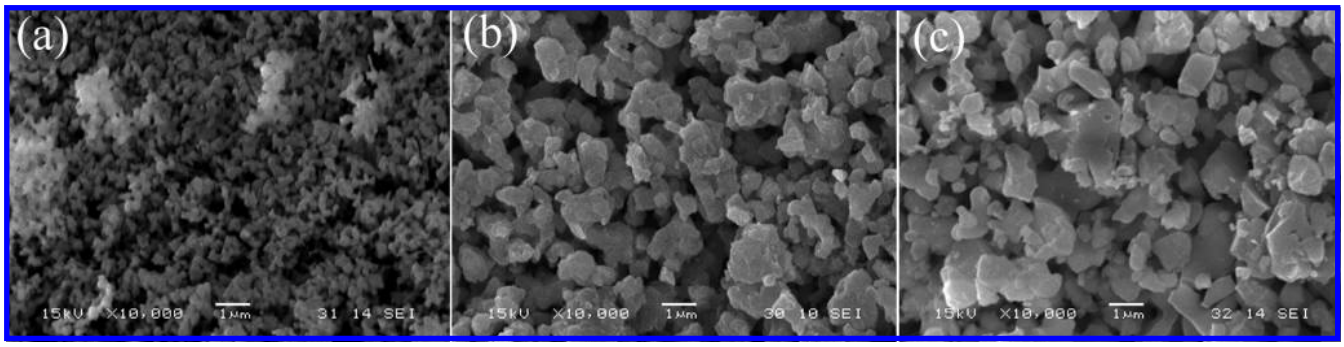

Figure 11. SEM micrographs of (a) Fap, (b) 25ZnAp, and (c) 50ZnAp samples after calcination at 900 °C.

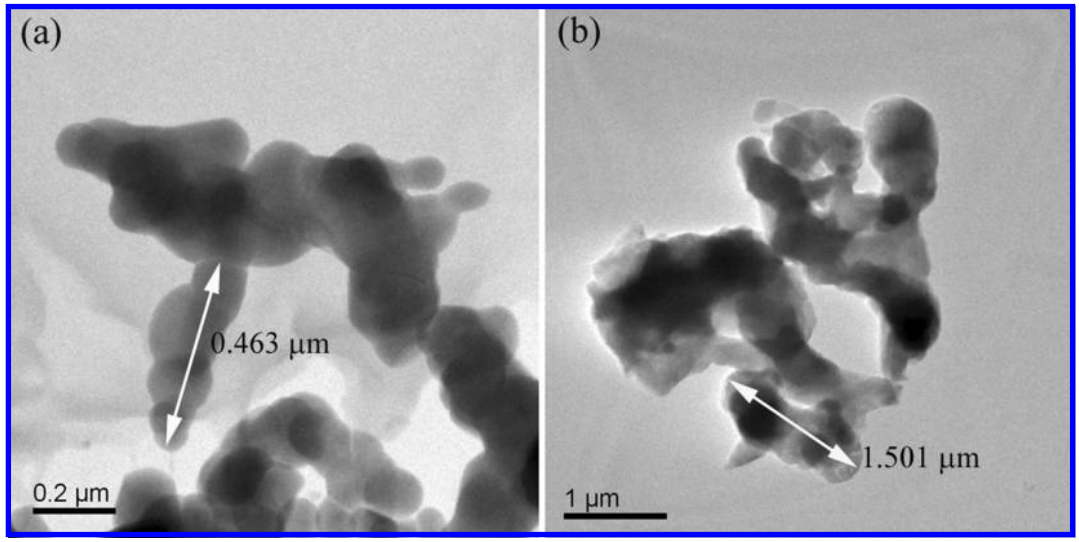

Figure 12. BF micrographs of calcined samples: (a) Fap; (b) 25ZnAp.

According to HRTEM, the bulk of the Fap particles had crystalline nanostructures while 25ZnAp consisted of microparticles of bulk amorphous characteristics. The randomness of the lattice fringes observed in the nanostructures of 25Znap and 50ZnAp further suggests the high amorphous characteristics of the samples. The high Ca/P molar ratio observed for 25ZnAp sample (Table 4) further verifies the presence of the amorphous characteristics in the sample. For 50 ZnAp, however, a lower Ca/P molar ratio was observed because the sample contained two chemical phases. In the case of the 75ZnAp and the ZnAp samples, the different morphologies confirmed the nonfluorapatite chemical phases identified with respect to the samples containing the fluorapatite phase.

The linear increase in the weight losses with zinc identified by TGA implies a low thermal stability with respect to high zinc levels. This thermal behavior is also supported by the formation of secondary phases such as ammonium zinc phosphate and zinc phosphate and is confirmed by calcination observations. Calcined Fap contained only the fluorapatite phase, but in the 25ZnAp sample a secondary chemical phase was identified. On the other hand, 50ZnAp did not have any fluorapatite phase after calcination. These results suggest that zinc lowered the integrity of the thermally stable fluorapatite phase. Possible reasons for the low thermal stability of zinc-substituted fluorapatite would be the repelling effects of low radii zinc ions from some of the cationic locations in the fluorapatite structure because of incompatible ionic radii and the formation of low-melting zinc-incorporated chemical phases as secondary phases when heating the samples. TEM images of the calcined Fap and calcined 25ZnAp also showed some similar characteristics even though the latter had two chemical phases. HRTEM imaging illustrated that the zinc incorporation into some areas of the fluorapatite structure is random and some areas have a particular order. Lattice fringe displacements and randomly missing atomic details in the HRTEM image in Figure 14b also suggest that zinc substitutions are difficult to achieve in the fluorapatite structure in a complete manner.

Sintering of the first two samples in Table 1 also verified some important findings about the as-synthesized and the calcined samples. Results showed the first two as-synthesized samples to have the highest thermal stability while the other three samples melted in the sintering process because of the presence of low-melting zinc phosphates. The fluroapatite phase in the as-synthesized Fap and 25ZnAp samples remained after sintering at 1200 °C but with the formation of a secondary phosphate phase. However, the phase-pure fluorapatite of the calcined Fap had the highest chemical phase stability because the zinc-incorporated fluorapatite phase in the calcined 25ZnAp sample decomposed completely after it was sintered. XRD and TEM studies explain why the 25ZnAp sample has a lower thermal stability than Fap. The amorphous character

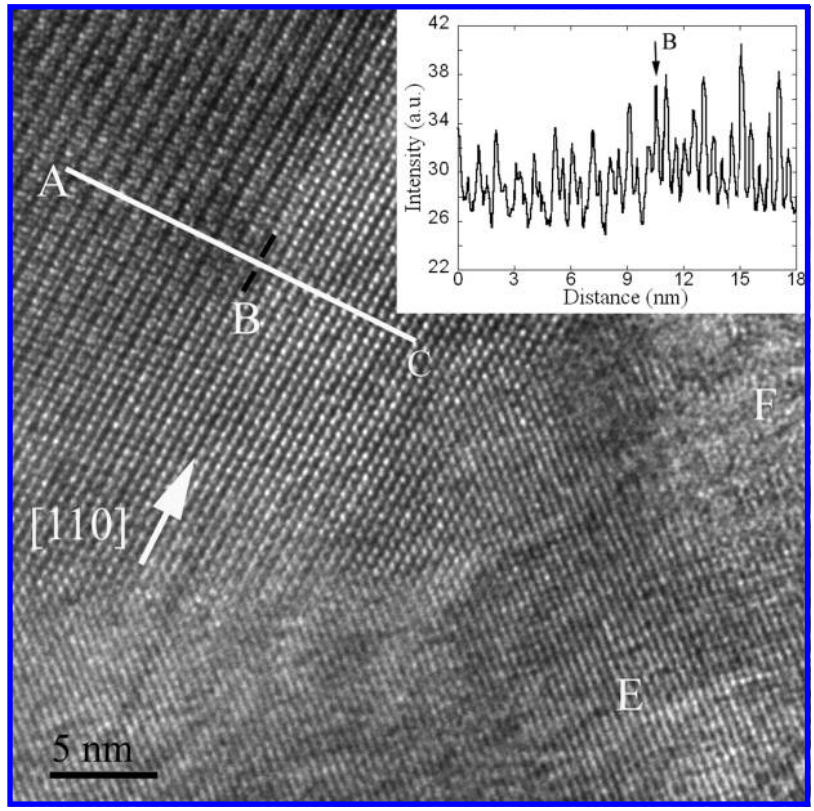

Figure 13. HRTEM image of 25ZnAp after calcination at 900 °C. Inset is the intensity profile obtained from along the line A to C.

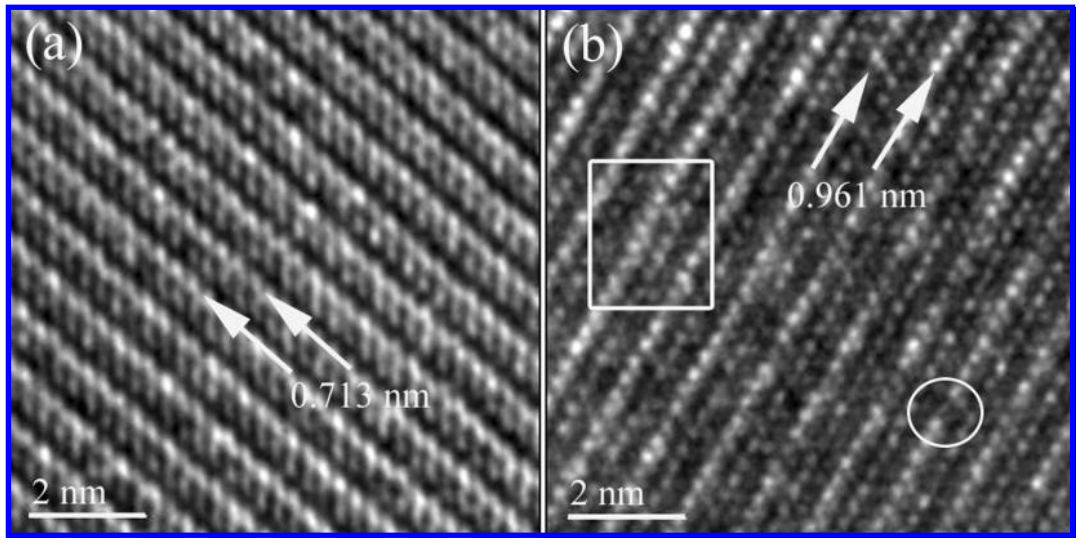

Figure 14. HRTEM images of the calcined (a) Fap and (b) 25ZnAp samples showing their structure details.

identified in 25ZnAp macroscopically and microscopically was probably due to an excess zinc level which cannot be incorporated into the fluorapatite structure. Therefore, when calcining the sample any loosely bound and excess zinc prefers to come out as a secondary phosphate phase ($CaZn_2(PO_4)_2$) rather than staying as the zinc-substituted fluorapatite phase. However, the removal of this phase resulted in the removal of some of the atomic layers in the zinc-substituted fluorapatite phase making it vulnerable to sintering. A complete decomposition of the fluorapatite phase was thus observed in the 25ZnAp sample further confirming the presence of the zinc-substituted fluorapatite in the as-synthesized sample.

5. Conclusion

Substitution of calcium in fluorapatite by zinc is possible and is demonstrated to be concentration dependent. The phase purity of fluorapatite in the samples decreases with the increase in zinc substitution since random incorporation of zinc is no longer effective for large quantities of zinc. A 25 mol % of zinc substitution leads to a single-phased fluorapatite, but the formation of a secondary phase was identified

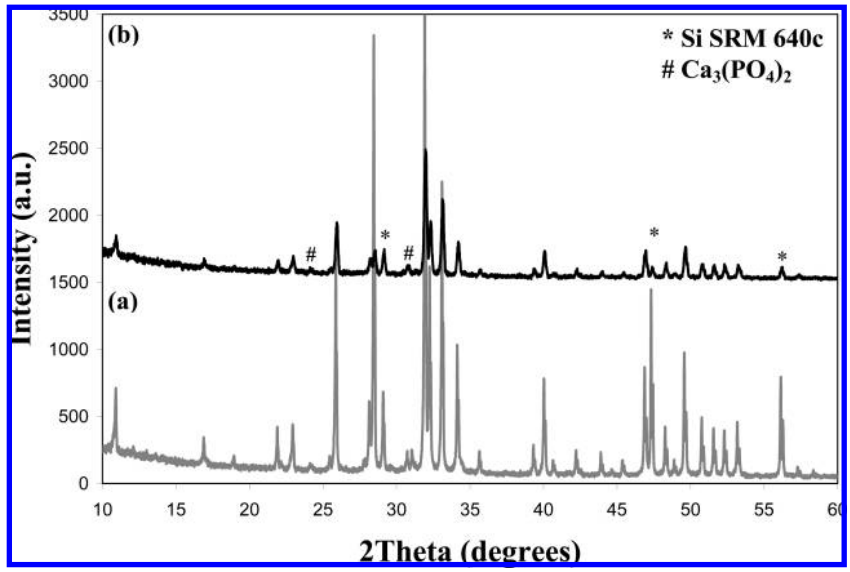

Figure 15. XRD pattern comparison of sintered Fap samples: (a) as-synthesized sample after sintering; (b) calcined sample after sintering.

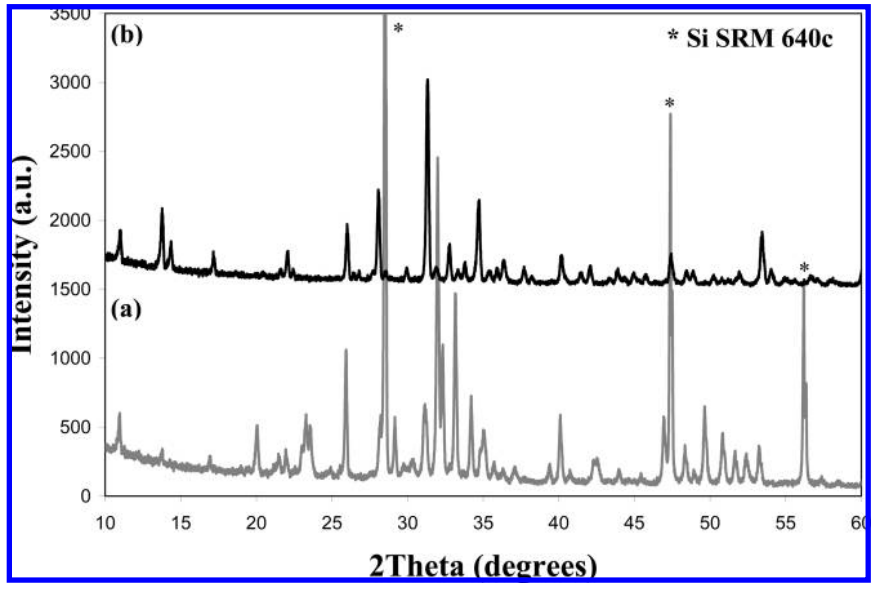

Figure 16. XRD pattern comparison of sintered 25ZnAp samples: (a) as-synthesized sample after sintering; (b) calcined sample after sintering.

when the zinc level increased to 50 mol %. A fluorapatite phase could not be identified in samples with 75 mol % and 100 mol % of zinc substitutions probably because of the repelling effects of large quantities of zinc in the competition to find locations in atomic coordinates of fluorapatite structure, forming other favorable chemical phases such as zinc phosphates. The two samples, synthesized using 25 mol % and 50 mol % of zinc showed some similar morphological and microstructural properties to that of single-phased fluorapatite (Fap). However, nanostructural characteristics similar to Fap were identified only in the 25ZnAp sample. The 50ZnAp sample showed a lower thermal stability which is likely due to the instability of the zinc-incorporation into the fluorapatite nanostructure and the secondary phases identified in the sample. The sintering properties of the as-synthesized 25ZnAp sample are similar to the as-synthesized Fap sample. However, a complete decomposition of the zinc-incorporated fluorapatite chemical phase in the calcined 25ZnAp sample resulted indicating a lower thermal stability than a single-phased fluorapatite. Amorphous characteristics identified in the as-synthesized samples both by XRD and by HRTEM and the dislocations in the atomic arrangement or discrete space fillings in the nanostructure of the sample are the probable reasons for the thermal instability of the zinc-substituted fluorapatite.

Acknowledgment. The authors would like to thank Drs. Anthony Hechanova and Clay Crow at UNLV for their support. We also thank Dr. Longzhou Ma at the TEM facility of the Harry Reid Center for Environmental Studies and Dr. Thomas Hartman at Idaho State University. This research is funded by the United States Department of Energy Grant DE-FG-04-2001AL67358 (AAA - Fluorapatite - Task 16).

IC800794X